

Phase I Final Report

SERRI Project: Biosensor Research

**Project Principal Investigator:
Dr. Andrienne C. Friedli**

This material is based upon work supported by the U.S. Department of Homeland Security under U.S. Department of Energy Interagency Agreement 43WT10301. The views and conclusions contained in this document are those of the authors and should not be interpreted as necessarily representing the official policies, either expressed or implied, of the U.S. Department of Homeland Security.

SERRI Project: Biosensor Research (81100)

PHASE I FINAL REPORT

Dr. Andrienne C. Friedli

Dr. William M. Robertson

Dr. Stephen M. Wright

Date Published:

December 2009

Submitted by Middle Tennessee State University

Prepared for
U.S. Department of Homeland Security
under U. S. Department of Energy Interagency Agreement 43WT10301

Prepared by
OAK RIDGE NATIONAL LABORATORY
Oak Ridge, Tennessee
managed by
UT-BATTELLE, LLC
for the
U.S. DEPARTMENT OF ENERGY
under contract DE-AC05-00OR22725

CONTENTS

LIST OF FIGURES	v
LIST OF TABLES	v
ACRONYMS	vii
SOUTHEAST REGION RESEARCH INITIATIVE	ix
1. INTRODUCTION	1
1.1 Objective	1
1.2 Significance.....	1
1.3 Relevance to the Department of Homeland Security (DHS).....	1
1.4 Improvement of DHS Capabilities.....	2
2. PROJECT TEAM AND WORKFORCE DEVELOPMENT	2
2.1 Personnel	2
2.2 Presentations	3
3. ACCOMPLISHMENTS	4
3.1 Develop an Affinity–Binding Based Flow Biosensor (Task 1)	4
3.1.1 Device Configuration.....	4
3.1.2 Multilayer Design and Targeted Sensing.....	6
3.1.3 Biological Targets	7
3.1.4 Sensing Infectious Agents	11
3.2 Develop Gas- and Vapor-Sensitive Layers for a SEW Flow Sensor (Task 2)	12
3.2.1 Multilayer Design.....	12
3.2.2 Calculated Refractive Index Sensitivity in Polymeric Materials.....	13
3.2.3 Terminal Layer Design	14
3.2.4 Ormosil Synthesis.....	14
3.2.5 Substrate Surface Cleaning Method.....	16
3.2.6 Film Formation	16
3.2.7 Template Removal and Reabsorption	16
3.2.8 Imprinted Ormosil Characterization	16
3.2.9 Effect of Film Environment Upon DNT Sensing.....	17
3.2.10 Film Selectivity for DNT.....	19
3.2.11 Nonselective Gas and Vapor Sensing with the SEW Sensor	19
3.3 Develop Strategies for Compact Sensors (Task 3)	20
3.4 Quantification of Sensitivity	21
4. SUMMARY	22
5. REFERENCES	22

LIST OF FIGURES

1. Flow cell configuration	5
2. Optical configuration required to generate and detect surface SEWs	5
3. Shift in coupling angle (measured in pixels) versus time	6
4. <i>Bacillus atrophaeus</i> endospore stain.....	8
5. Scanning electron micrograph of <i>B. pumilus</i> endospores.....	9
6. Fluorescence detection of endospores	9
7. Fluorescence image of a 5 × microarray of endospores.....	10
8. Antibody trapping of endospore (biosensor)	10
9. Biosensor surface mode shift due to exposure to <i>B. atrophaeus</i>	11
10. Spore-antibody reaction experiment showing selective binding	12
11. Calculated surface optical wave penetration into the air interface in two PBGMs.....	13
12. Calculated angular mode shift in a 700 nm thick OV-225 film	14
13. Cartoon showing nanocavity with DNT template.....	14
14. Synthesis of ormosil polymer	15
15. Reagents from Table 3.....	15
16. UV spectra of film templated with DNT	17
17. Effect of film environment upon extraction of DNT	17
18. Effect of film environment upon absorption of DNT vapor.....	18
19. Effect of film environment on percentage of DNT in the film after extraction and reabsorption.....	18
20. Spartan electrostatic potential density maps for molecules of similar shape (DMT) and polarity (DNB) to DNT.....	19
21. Vapor binding results for isopropanol, acetone, acetic acid, and ether	20
22. Schematic of a compact portable SEW sensor configuration	21

LIST OF TABLES

1. Endospore Enumeration.....	8
2. Antibody Binding with Endospores	10
3. Reagents and Conditions for Synthesis of Sol-Gels.....	15

ACRONYMS

ATCC	American Type Culture Collection
BSA	bovine serum albumin
CCD	charge-coupled device
dH ₂ O	deionized water (H ₂ O)
DHS	Department of Homeland Security
DMT	2,4-dimethoxytoluene
DNB	2,2'-dinitrobiphenyl
DNT	2,4-dinitrotoluene
HeNe	helium neon (as in helium neon laser)
MTSU	Middle Tennessee State University
NB	3-nitrobiphenyl
ormosil	organically modified silicate
PBG	photonic bandgap
PBGM	photonic bandgap multilayer
PBS	phosphate buffered saline
PI	principal investigator
PTMOS	phenyl trimethoxysilane
RI	refractive index
RIU	refractive index unit
RT	room temperature
SDS	sodium dodecyl sulfate
SEM	scanning electron microscope
SEW	surface electromagnetic wave
SP	surface plasmon
TEOS	tetraethoxysilane
TMOS	tetramethoxysilane
USB	universal serial bus
UV	ultraviolet
λ_{\max}	wavelength value corresponding to maximum absorbance

SOUTHEAST REGION RESEARCH INITIATIVE

In 2006, the U.S. Department of Homeland Security commissioned UT-Battelle at the Oak Ridge National Laboratory (ORNL) to establish and manage a program to develop regional systems and solutions to address homeland security issues that can have national implications. The project, called the Southeast Region Research Initiative (SERRI), is intended to combine science and technology with validated operational approaches to address regionally unique requirements and suggest regional solutions with potential national implications. As a principal activity, SERRI will sponsor university research directed toward important homeland security problems of regional and national interest.

SERRI's regional approach capitalizes on the inherent power resident in the southeastern United States. The project partners, ORNL, the Y-12 National Security Complex, the Savannah River National Laboratory, and a host of regional research universities and industrial partners, are all tightly linked to the full spectrum of regional and national research universities and organizations, thus providing a gateway to cutting-edge science and technology unmatched by any other homeland security organization.

As part of its mission, SERRI supports technology transfer and implementation of innovations based upon SERRI-sponsored research to ensure research results are transitioned to useful products and services available to homeland security responders and practitioners.

For more information on SERRI, go to the SERRI Web site: www.serri.org.

1. INTRODUCTION

1.1 Objective

The objective of the project is to refine the design of an efficient, highly sensitive, inexpensive, and versatile sensor to detect potential biological and chemical hazards and apply it to specific biological and chemical hazards in real time.

The goal is to develop the sensor in its flow configuration and apply it to detect specific gases or vapors and hazardous biological species in solution. The sensor will be optimized for two test materials that are relevant to common biological and chemical weaponry: pathogenic spores and explosives.

1.2 Significance

In this project an optical flow cell biosensor previously developed at Middle Tennessee State University (MTSU) was modified and improved to detect specific established biological and chemical hazards. Several model endospores were used to mimic the behavior of anthrax, a bioterror agent, and dinitrotoluene, a model for the common explosive trinitrotoluene. Real-time sensing of both biological and chemical hazards at low concentrations from natural and man-made disasters is a potentially important analytical tool and preventative measure. Hoaxes or other terror tactics can alarm the public unnecessarily, so sensors are also important for rapid confirmation when threat agents are *not* present.

Chemical and biological agents are real and current threats to national security. Anthrax, the acute and often lethal disease caused by the pathogenic bacterium *Bacillus anthracis*, is considered to be the single greatest biological warfare threat (Buckeridge et al., 2006). The World Health Organization estimated that an aerial spray of bacterial endospores for 100 km could produce mortality rates as high as 50% extending 160 km downwind (Buckeridge). Even a 1-day delay in the treatment of those infected and the initiation of chemoprophylaxis to the masses could result in thousands of additional deaths and millions of dollars in expenditures (Cieslak and Eitzen, 1999). Therefore, it is imperative that a rapid, cost-effective method to detect and differentiate *B. anthracis* endospores from other nonvirulent species be developed.

Security at transportation hubs such as airports has been visibly tightened since 2001, yet the safety of the large amount of cargo entering U.S. ports has been questioned (Elias, 2007). As recently as Christmas 2009 a terrorist attempted to blow himself up aboard an aircraft bound for Detroit from Nigeria using explosives hidden within his clothing. New methods for real-time sensing of explosives residues are necessary to keep up with the moving target of terrorist activities.

1.3 RELEVANCE TO THE DEPARTMENT OF HOMELAND SECURITY (DHS)

Improved biochemical sensors capable of detecting trace amounts of specific infectious agents and/or environmental contaminants are key elements in applications relevant to community resilience following a natural disaster. Specific application examples include water quality assessment, biological threat detection, food safety, and medical diagnostics.

An interdisciplinary research team at MTSU has developed a novel photonic sensor based on surface electromagnetic waves (SEWs) generated in photonic bandgap multilayer (PBG) coated substrates. Sensing is accomplished by measuring the shift in the SEW resonance when dielectric conditions at the PBGM surface change (e.g., through antibody-antigen binding). The technique is similar to sensors based on the phenomenon of surface plasmon (SP) resonance. SP resonance sensors have a long and successful history in biosensing but have inherent application limitations.

1.4 Improvement of DHS Capabilities

The SEW sensor developed at MTSU improves on existing SP sensors in four significant ways.

1. *High sensitivity.* Both the SP and the SEW sensor are based on the resonant excitation of surface waves. However, the resonance width of the SEW mode is almost two orders of magnitude sharper than SP resonance with a concomitant increase in sensitivity.
2. *Operation at any wavelength.* SPs are generated in metal films. The operating wavelengths at which SP sensors can be made are limited by the intrinsic optical properties of the metal used. In general SP sensors are limited to wavelengths in the red and infrared. In contrast, SEWs are generated in PBGMs that can be designed and engineered to support SEWs at any wavelength.
3. *Chemical and physical robustness.* The metal films used for SP sensors are mechanically soft, and many of the best metals for SP generation (e.g., silver) are too chemically reactive to make practical sensors. PBGMs eliminate these problems; the multilayers can be made from a wide variety of dielectric materials and are chemically and mechanically very stable. Furthermore, the multilayers can be made in large quantities using commercially available thin film deposition techniques.
4. *Versatile platform for designing a wide variety of sensors.* The terminating layer of the PBGM can be almost any dielectric. We chose glass (SiO₂) as the terminating layer because the technology for binding biomolecules to glass surfaces is well developed.

During Phase I of the SERRI-supported project the principal investigators (PIs) sought to advance knowledge in optical sensing in three ways: (1) producing a flow cell based sensor that targets a number of important public health or biothreats; (2) extending the SEW technique to perform gas sensing using spin-coated layers containing pores or nanocavities as the terminating layer of the PBGMs; and (3) designing, prototyping, and testing compact portable sensor instruments to move the SEW sensing technique from the optics laboratory to a form usable in practical sensing situations.

2. PROJECT TEAM AND WORKFORCE DEVELOPMENT

2.1 Personnel

The project was carried out by an interdisciplinary team consisting of three faculty members and six undergraduate students from the Departments of Chemistry, Biology, and Physics at MTSU. The project team consisted of the following.

Dr. Andrienne C. Friedli, Professor of Chemistry (PI)

Dr. Stephen M. Wright, Professor of Biology (co-PI)

Dr. William M. Robertson, Professor of Physics (co-PI)

Brandon Cathey, BS Student, Physics and Chemistry

Peter J. Cothron, BS Student, Chemistry

Merranda D. Holmes, BS Honors Student, Biology

Ja'be G. Kiri, BS Student, Biochemistry

Bart A. Morris, BS Student, Chemistry and Physics

Shannon B. Murphy, BS Honors Student, Biology

Thomas A. Standley, BS Student, Chemistry and Biology

The project team operated as three collaborating subgroups, each headed by a faculty mentor (co-PI). The co-PIs interacted regularly to plan and perform experiments, analyze data, and prepare reports. Some students worked across disciplinary barriers, performing experiments in two laboratories. Students participating in the project gained knowledge and experience in surface chemistry, physics of optics, molecular biology as applied to immunosensing (spore/antibody), and gas sensing. All have presented at least once at local, regional, or national venues, and all are undergraduate students planning to work in science, technology, engineering, or mathematics.

2.2 Presentations

Kara D. Cole, Peter J. Cothron, Cory L. Davis, Thomas A. Standley, and Andrienne C. Friedli. "Nanoimprinted Organosilicates for Detection of Aromatic and Nitroaromatic Compounds." 237th National Meeting of the American Chemical Society, March 22–26, 2009, Salt Lake City, UT. Abstract CHED 247. (Poster)

Merranda D. Holmes and Stephen M. Wright. "The Production, Quantification and Fluorescent Detection of Anthrax-Simulating Endospores." Presented at the 118th Meeting of the Tennessee Academy of Science, Nashville, November 20–22, 2008.

Ja'be G. Kiri, and Andrienne C. Friedli. "Modified Organosilicates as Potential Carbohydrate Sensors." University-Wide Scholars Day, April 3, 2009, Middle Tennessee State University, Murfreesboro, Tennessee (Poster 168).

Ja'be G. Kiri and Andrienne C. Friedli. "Nanoimprinted Organosilicates for Selective Detection of 2,4-Dinitrotoluene Explosives Model." TLSAMP (Tennessee Louis Stokes Alliance for Minority Participation), November 2009, Nashville (Talk).

Shannon B. Murphy and Stephen M. Wright. "A Label-Free Method for Detection and Differentiation of *Bacillus spp.* Endospores." Presented at the 119th Meeting of the Tennessee Academy of Science, Knoxville, October 29–30, 2009.

Bart A. Morris, Peter J. Cothron, Kara D. Cole, Cory L. Davis, Andrienne C. Friedli, and William M. Robertson. "Organosilicate Films Coupled to Photonic Band Gap Multilayer Materials for Gas Sensing." University-Wide Scholars Day, April 3, 2009, Middle Tennessee State University, Murfreesboro, Tennessee (Poster 112).

Peter J. Cothron, Kara D. Cole, Cory L. Davis, Thomas A. Standley, and Andrienne C. Friedli. "Nanoimprinted Organosilicates for Detection of Aromatic and Nitroaromatic Compounds." University-Wide Scholars Day, April 3, 2009, Middle Tennessee State University, Murfreesboro, Tennessee (Poster 103).

3. ACCOMPLISHMENTS

During the first phase of the project three key areas were investigated: (1) producing a flow cell based sensor that targets a number of important public health or biothreats; (2) extending the SEW technique to perform gas sensing using spin-coated layers containing pores or nanocavities as the terminating layer of the PBGMs; and (3) designing, prototyping, and testing compact portable sensor instruments to move the SEW sensing technique from laboratory to production scale.

Below is a detailed accounting of each of the three key areas, which correspond to the three tasks described in Sect. 1.4.

3.1 Develop an Affinity–Binding Based Flow Biosensor (Task 1)

In work completed before SERRI funding, we demonstrated that a flow cell configuration could be used to detect the shift of the SEW mode when affinity binding (e.g., antibody-antigen) occurs on suitably prepared PBGMs (Robertson, 2005). The amount of the angular shift of the SEW mode is proportional to the quantity of material that binds to the surface. This method is very effective in detecting relatively small target molecules (i.e., small compared to the wavelength of the light) and potentially useful for quantifying the amount of target material in the sample under test. However, many important applications in food safety, water quality, and biothreat detection involve the detection of spores or bacteria, which are larger than the wavelength of light used to generate SEWs. In these cases the effect of binding is to destroy the SEW mode. We have two strategies to create a SEW sensor for large entities. The first is to simply use the disappearance of the mode when exposed to a test sample as evidence that the specific binding target entity (e.g., a spore) is present. The second method is to move to a longer wavelength and to redesign the multilayer so that the surface mode is not destroyed by the binding of a large entity. The first method was the primary focus in this research.

3.1.1 Device Configuration

The basic optical configuration for coupling and detecting SEW resonance is the same for both the biosensing and gas/vapor sensing applications. In each case a prism is used to couple laser light at 635 nm into SEWs at the surface of a multilayer structure. The multilayer is enclosed in a flow cell configuration. In the case of biosensing, the flow cell is set up to allow liquid flows to monitor bioreactions between the sensitized multilayer and spores or proteins in solution/suspension. For vapor sensing, gas is flowed through the cell,

either as a carrier to propel vapor samples or as the material to be sensed directly. The multilayer design for each application is different as described in more detail in the sections below.

Figure 1 shows the structure of the flow cell. The flow cell and the attendant optical components necessary to generate and detect coupling to SEWs are shown in Figure 2.

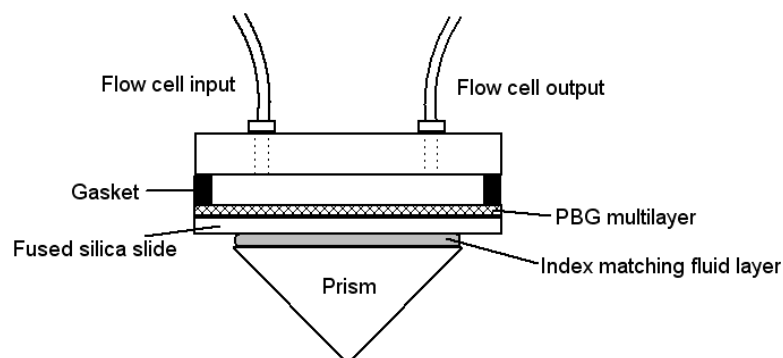


Figure 1. Flow cell configuration.

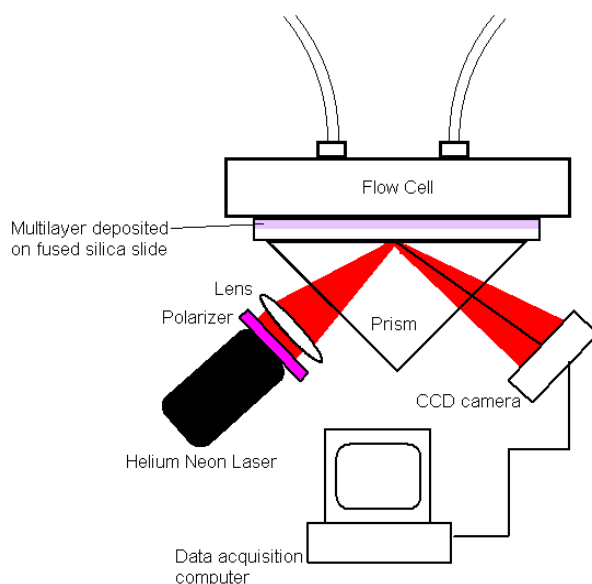


Figure 2. Optical configuration required to generate and detect surface SEWs.

The multilayer structures are deposited on one side of glass slides. The flow cell is constructed by placing a gasket on top of the multilayer and then compressing the gasket with the flow unit machined out of Plexiglas and containing input and output ports. The reaction volume lies between the multilayer and the flow unit, and its size is determined by the thickness of the gasket.

The flow cell is optically connected to the prism using index matching fluid. Polarized laser light is coupled into the SEW mode using a lens to focus the light through the prism. The light is focused to a small point at the multilayer surface. The focused light is incident over a range of angles; however, only one small band of angles couples to the SEW mode at the multilayer surface. The light that couples to the SEWs is lost from the reflected light. The

reflected beam consists of a uniformly bright field with a dark line through it at the angle of SEW coupling. As conditions at the surface change due to reactions with the sensitized multilayer, this coupling angle varies. Tracking the change in coupling angle is the basis of sensing action. The angle of the mode coupling is monitored by imaging the reflected beam onto a CCD (charge-coupled device) array. The CCD image is captured by the data acquisition computer through a USB connection. The computer analyzes the captured image and determines the shift in the SEW mode in terms of the number of pixels that the mode has moved from its original position on the CCD. The control and data acquisition program is written in MATLAB. Typical flow cell experiments consist of measuring the mode coupling angle as a function of time. As an example of the angle shift versus time, Figure 3 shows flow cell data with pure water alternating with water-ethanol mixtures of four different concentrations. The slightly different refractive index (RI) of the water-ethanol mixtures causes the SEW conditions to change sufficiently to create a coupling angle shift.

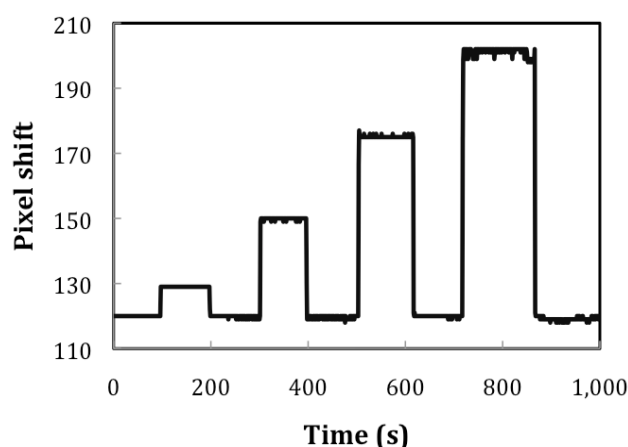


Figure 3. Shift in coupling angle (measured in pixels) versus time. The baseline is pure water, and pixel shifts occur with the introduction of 0.5%, 1.5%, 2.5%, and 3.5% ethanol-water mixtures at 100 s, 300 s, 500 s, and 700 s, respectively.

3.1.2 Multilayer Design and Targeted Sensing

The multilayer design for the gas sensing and the biosensing applications and the means by which they are sensitized are described briefly in this section. The coupling of light to SEWs occurs only when the light is incident above the angle for total internal reflection between the first medium (prism) and the last medium (flow cell). Thus, there is a different multilayer design for the gas and liquid flow cell configurations. For the liquid flow system used in biosensing experiments, the multilayer of alternating TiO_2 and SiO_2 layers is designed (Robertson, 2008; Shinn, 2005) to exhibit a SEW mode at an angle just a few degrees above total internal reflection. This multilayer is manufactured commercially. To make it sensitive to a specific entity the multilayer is first chemically coated with an amine or epoxy-terminated silane to allow the binding of biomolecules, and then an antibody appropriate for the target species is applied.

3.1.3 Biological Targets

3.1.3.1 Organisms used

Due to the virulent nature of *B. anthracis*, bioweapon studies have been confined to a limited number of specialty laboratories. However, using nonvirulent model organisms of comparable spore size and genetic relationship to anthrax may lead to the most applicable results in the safest manner. *Bacillus atrophaeus* and *B. thuringiensis* are two anthrax simulation organisms identified in the literature (Buckeridge). The organisms used in this study included *B. atrophaeus* [American Type Culture Collection (ATCC) number 9372], *B. thuringiensis* (ATCC number 10792), and *B. pumilus* (ATCC number 700814). *Bacillus pumilus* has not been routinely used as a simulant for *B. anthracis* and was originally chosen for this study as an endospore “outlier” which was not expected to react with antibodies to other *Bacillus* spp. As noted later in this report, *B. pumilus* was determined to have characteristics that suggest it would be an appropriate model for anthrax. Thus additional study was undertaken with *B. pumilus*. *Streptococcus pyogenes* was selected as a negative control because it has no relation to any of the *Bacillus* spp. and, as a coccus bacterium, is about the same size as a *Bacillus* endospore, 0.6–1.0 μm (Joklik et al., 1988). A second negative control endospore-forming organism, *Clostridium sporogenes* (ATCC number 3584), was also studied.

3.1.3.2 Endospore preparation

Having a reliable method for endospore preparation is the initial step in the evaluation of any detection process. One of the goals of this research was to develop a protocol for the consistent production of endospores. The organisms were inoculated into 5 mL tryptic-soy broth and incubated overnight at 35°C. From each broth 100 μL was spread on nutrient-deficient AK Agar number 2 plates. The plates were incubated at 30°C and harvested on days 4, 6, 8, and 10 (*B. atrophaeus*, *B. pumilus*, and *C. sporogenes*) or days 14, 16, 18, and 20, post-inoculation (*B. thuringiensis*). After appropriate incubation, 10 mL cold phosphate buffered saline (PBS) was added to the plate, and endospores were scraped off using a sterile loop. Endospore stains were prepared, and a visual inspection of sporulation was recorded during this process to determine optimum sporulation. The endospore-PBS suspension was transferred to a 15 mL centrifuge tube and centrifuged for about 15 minutes. The PBS was decanted, and the pellet was resuspended in 1 mL sterile deionized H₂O (dH₂O) and transferred to a 1.5 mL tube. The tube was spun in a microcentrifuge for 5 minutes at 13,000 rpm. The dH₂O was decanted and the endospores were resuspended in 1 mL fresh dH₂O at room temperature (RT). This endospore-dH₂O suspension was heated at 65°C in a heat block for 45 minutes to kill remaining vegetative cells and served as the endospore stock for the subsequent experiments.

3.1.3.3 Endospore stain

A loopful (about 4–5 μL) of each endospore preparation was applied to a standard microscope slide and spread out to a diameter between 1 and 1.5 cm. The slide was air-dried and heat fixed by passing the slide over a flame. The slide was flooded with malachite green stain and steamed by passing the slide over a Bunsen burner for 3 to 5 minutes. Malachite green was continually added to the slide to prevent drying out. The slide was allowed to

cool and then rinsed with tap water for 30 seconds. Safranin was added to the slide and allowed to counterstain for 1 minute. The slide was then rinsed with tap water for 5 seconds and blotted dry. The slide was evaluated using a light microscope under oil immersion. Endospores appeared green and vegetative cells appeared pink using this preparation method, as pictured in Figure 4.

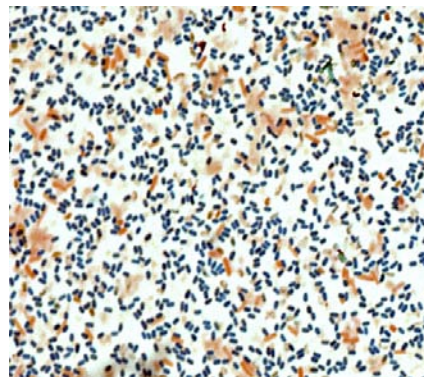


Figure 4. *Bacillus atrophaeus* endospore stain. Sporulation was estimated to be 90%.

3.1.3.4 Endospore enumeration

A dilution series was prepared for 10^5 – 10^{12} depending on the density of the endospore preparation for each organism. Fifty μL of each dilution was applied to a tryptic soy agar plate, spread using a sterile bent glass rod, and incubated overnight at 30°C . The viable endospore count was determined as (number of colonies on a plate) \times (total dilution of the plate). Total endospore counts (viable and nonviable) were made by direct counts using a hemacytometer. These processes were repeated three times and averaged to give a final average concentration of the original stock. Results are shown in Table 1.

Table 1. Endospore Enumeration

Organism (optimum day)	Plate Count	Total Count	Viability (%)
<i>B. atrophaeus</i> (8)	$8.667 \pm 0.291 \times 10^9$	$1.376 \pm 0.141 \times 10^{10}$	63
<i>B. pumilus</i> (8)	$1.375 \pm 0.065 \times 10^{10}$	$1.775 \pm 0.081 \times 10^{10}$	77
<i>B. pumilus</i> (8)	$2.920 \pm 0.192 \times 10^{10}$	$4.582 \pm 0.424 \times 10^{10}$	64
<i>B. thuringiensis</i> (16)	$6.985 \pm 0.138 \times 10^8$	$1.192 \pm 0.110 \times 10^9$	59
<i>C. sporogenes</i> (6)	$1.02 \pm 0.136 \times 10^9$	$2.809 \pm 0.144 \times 10^9$	36

3.1.3.5 Scanning electron microscopic analysis

One microliter of each dilution from each endospore-forming organism was placed directly on the surface of a scanning electron microscope (SEM) aluminum specimen stage and coated with an 8 nm layer of gold. Micrographs were taken of each sample at an accelerated voltage between 15 and 20 kV. These micrographs were used to determine morphological variation among the *Bacillus* spp. Image J software was used to measure spores individually, and a dimensional range was established for each endospore. About 20 endospores of each species were measured, and an average was taken. Endospores of *B. pumilus* are shown in the electron micrograph in Figure 5.

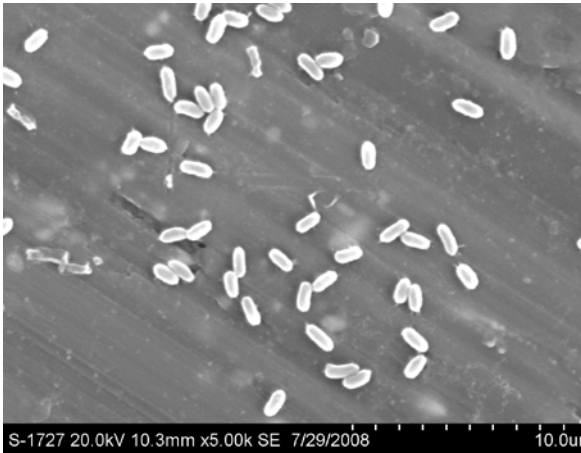


Figure 5. Scanning electron micrograph of *B. pumilus* endospores.

For an endospore to be considered an acceptable simulant for *B. anthracis*, it should have similar dimensions and endospore coat properties. Previous studies have reported that the spore diameter for *B. anthracis* is between $0.81 \pm 0.08 \mu\text{m}$ and $0.86 \pm 0.08 \mu\text{m}$ (Carrera et al., 2006). The length of these spores fall into one of two categories: those with mean spore lengths of $1.26 \pm 0.13 \mu\text{m}$ or shorter, and those with mean spore lengths between 1.49 and $1.67 \mu\text{m}$. *Bacillus atrophaeus* and *B. thuringiensis* have been previously reported as acceptable size-based simulants for *B. anthracis*. This study's SEM analysis determined that *B. atrophaeus* endospores, harvested on day 8, have a mean length of $1.39 \pm 0.04 \mu\text{m}$ and width $0.77 \pm 0.01 \mu\text{m}$ under the conditions used. Previous studies report *B. atrophaeus* to have a mean length of $1.22 \pm 0.12 \mu\text{m}$ and width of $0.65 \pm 0.05 \mu\text{m}$ (Carrera). The slight discrepancies in measurement are likely due to minor variations in preparation conditions. *Bacillus pumilus* endospores from day 8 of this study had a mean length of $1.23 \pm 0.03 \mu\text{m}$ and a mean width of $0.58 \pm 0.01 \mu\text{m}$. There have been no reports of *B. pumilus* endospore dimensions. Endospores from *B. thuringiensis* (day 18) were found to have a mean length of $1.58 \pm 0.24 \mu\text{m}$ and width of $0.75 \pm 0.22 \mu\text{m}$, which is supported by previous studies reporting a mean length of $1.61 \pm 0.18 \mu\text{m}$ and a mean width of $0.80 \pm 0.07 \mu\text{m}$ (Carrera). These dimensional similarities with *B. anthracis* suggest that *B. atrophaeus*, *B. thuringiensis*, and *B. pumilus* seem to be acceptable nonpathogenic simulants for *B. anthracis* and may be used in developing anthrax detection technologies.

3.1.3.6 Microarray preparation and detection

Endospores were applied as microarrays with a SpotBot microarray robot. A volume of 2.8 nL was delivered to form each spot and the epoxy slide was allowed to dry at RT for at least 2 hours. The slide was heated at 95°C for 25 minutes to ensure endospores were bound tightly to the slide and then put into an ultraviolet (UV) cross-linker for two cycles ($6,500 \mu\text{J}/\text{cm}^2$) to inactivate remaining epoxy functional groups. The slide was washed with 0.1% SDS for 5 minutes, then with dH₂O for 2 minutes. All washes were performed in a slide washing chamber on a stir plate at 300 rpm without heat. Blocker was applied to the edge of the slide using 1 μL blocker per square millimeter of coverslip. The coverslip was placed over the blocker and the slide incubated in a moisture chamber at RT for 1 hour. The coverslip was removed and the same series of washes and spin drying were performed. The format for detection of endospores using a secondary fluorescently labeled antibody is depicted in Figure 6.

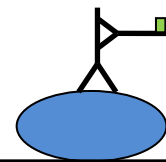
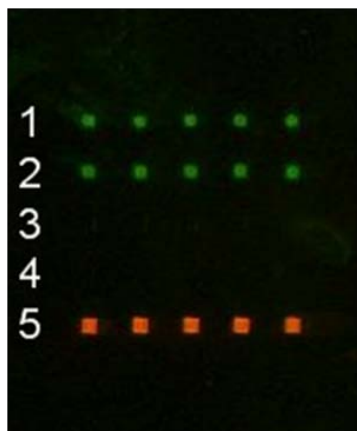


Figure 6. Fluorescence detection of endospores. The endospore (blue oval) is bound by a primary antibody (black Y-shaped structure), which is then bound by a secondary antibody with a fluorescent label (Y-shaped structure with green label).

A microarray of endospores was detected using monoclonal mouse anti-*B. atrophaeus* as the primary antibody (Figure 7). The secondary labeled antibody was goat anti-mouse containing Cy3, appearing green, indicating that binding occurred with both *B. atrophaeus* and *B. pumilus*.



Endospores applied as 5 × array

- Row 1 = *B. atrophaeus*
- Row 2 = *B. pumilus*
- Row 3 = *B. thuringiensis*
- Row 4 = *S. pyogenes*
- Row 5 = Immunoglobulin G, Cy5 label

Figure 7. Fluorescence image of a 5 × microarray of endospores.

A summary of antibody binding among the endospore-forming organisms appears in Table 2.

Table 2. Antibody Binding with Endospores

Organism	Polyclonal anti- <i>B. atrophaeus</i>	Monoclonal anti- <i>B. atrophaeus</i>	Monoclonal anti- <i>B. thuringiensis</i>
<i>B. atrophaeus</i>	+	+	-
<i>B. pumilus</i>	+	+	-
<i>B. thuringiensis</i>	+	-	+
<i>C. sporogenes</i>	-	-	-

Cross-reactivity among *Bacillus spp.* is common, in agreement with other studies (Quinlan and Foegeding, 1997). The use of monoclonal antibody, directed against a single conserved epitope, provides greater specificity as seen in the case of anti-*B. thuringiensis*. The binding of anti-*B. atrophaeus* monoclonal antibody with *B. pumilus* suggests that this organism may be an appropriate anthrax endospore simulant.

The scheme for detection of endospore presence in the absence of fluorescence is shown in Figure 8. This format is the basis for detection of endospores based on a SEW that occurs in photonic bandgap (PBG) coated substrates.

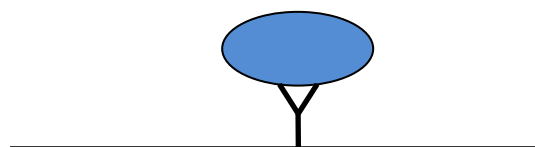


Figure 8. Antibody trapping of endospore (biosensor). A primary polyclonal antibody (black Y-shaped structure) is bound to a PBGM on a microscope slide. Binding occurs when the complementary antigen endospore (blue oval) is added to the slide.

3.1.4 Sensing Infectious Agents

The operation of the multilayer flow cell configuration for sensing bioreactions is illustrated in Figure 9 for binding spores to an anthrax simulant. This experiment is typical of the many we conducted in the course of this research and demonstrates sensing of a specific target species.

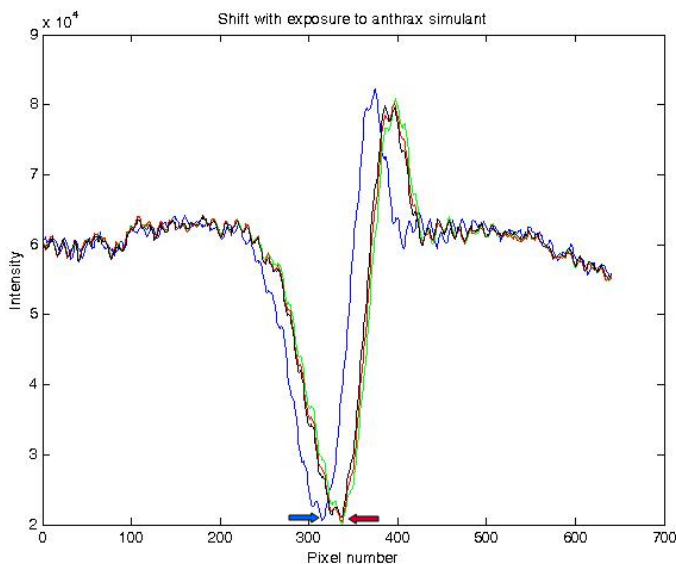


Figure 9. Biosensor surface mode shift due to exposure to *B. atrophaeus*. The blue line (blue arrow) shows the original surface mode at about 310 pixels. *Bacillus atrophaeus* endospores were injected into the system. The red and green lines (red arrow) illustrate the shift of the surface mode due to binding between the immobilized goat anti-*B. atrophaeus* antibodies on the slide and the injected endospores (about 330 pixels).

The PBGM was designed to exhibit a PBG at the frequency of the helium neon (HeNe) laser and at a range of angles above that for total internal reflection when the thickness of the termination layer was adjusted to set the surface optical wave resonance at an experimentally accessible angle. The multilayer was fabricated commercially and consisted of four bilayers of TiO₂ and SiO₂ (eight layers total) configuration. The first three bilayers were identical (128.5 nm TiO₂ and 199.7 nm SiO₂), and the last bilayer was 128.5 nm TiO₂ and 350 nm SiO₂. Calculations show that by adjusting the mode to be near the gap center the surface wave is strongly confined to the surface and sensitivity is maximized.

Experiments were conducted to demonstrate the detection of specific antibody-antigen binding and the determination of the rate kinetics of such reactions. For these experiments, bovine serum albumin (BSA) protein was coated onto the multilayer surface to bind to the anthrax-simulant endospores. The coated slide was mounted in the flow cell configuration as described above and the resulting SEW mode was found. Once the mode was found and transmitted to the CCD camera, no hardware was moved throughout the remainder of the experiments. The BSA treated slide was then exposed sequentially to various biological

agents by flushing them through the flow cell. The results from these experiments are documented in Figure 10.

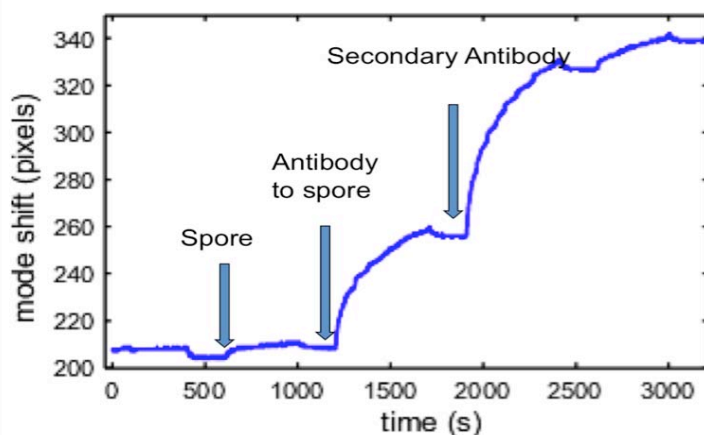


Figure 10. Spore-antibody reaction experiment showing selective binding.

The multilayer was exposed to a combination of substances—some with a specific binding affinity for the spore and some with no specific binding affinity to anything on the multilayer. Each time, 10 mL of solution was injected into the flow cell. BSA protein was first injected into the flow cell to act as a nonbinding control for the experiment. The data in Figure 10 show an unexpectedly weak change at 600 to 1,000 seconds, when solution containing *B. atropheus* was injected, but this effect went away when the flow cell was flushed with sterilized, distilled water. At 1,200 seconds rabbit anti-*B. atropheus* antibody was added, which binds to the spore that was previously injected. The binding of the antibody to the spore progressed from 1,200 to 1,700 seconds. At 1,700 seconds, water was flushed through the cell removing the excess antibody. Finally, the goat anti-rabbit antibody was added at 1,900 seconds. It should bind specifically to multiple sites on each rabbit anti-*B. atropheus* antibody molecule present on the slide as can be seen from the reaction between 1,900 and 2,400 seconds. There was one final null result binding experiment between 2,600 and 3,000 seconds. The experiment was designed to reveal the effects of two stages of binding. All other compounds were added as nonspecific binders to gauge the contributions of the change in index of the flow cell fluid as well as any nonspecific binding (e.g., hydrogen bonding) that may take place.

3.2 Develop Gas- and Vapor-Sensitive Layers for a SEW Flow Sensor (Task 2)

3.2.1 Multilayer Design

The standard SEW sensor operates by confining incident light in the outermost layer of the PBGM. Figure 11 illustrates the strong confinement of the surface wave just inside the PBGM and outside the surface when detecting relatively small molecules. The electromagnetic field of the SEW mode extends evanescently beyond the multilayer and detects dielectric loading by affinity binding at the surface. For the gas sensing experiments the last layer of the multilayer is the sensing medium. The multilayer is designed with a

series of TiO₂ and SiO₂ layers but with a lower index polymer as the terminating layer. The multilayer is fabricated commercially without the terminating organic layer.

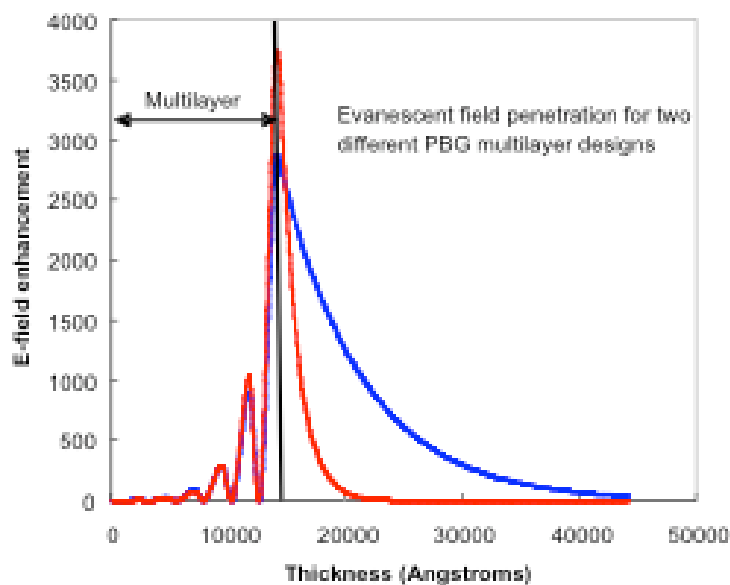


Figure 11. Calculated surface optical wave penetration into the air interface in two PBGMs. The multilayers were designed to detect films of thicknesses <50 nm (red line) and <5 μ m (blue line).

Before this project, an unexplored aspect of this phenomenon was the effect of changing the RI of the last SEW confining layer on the angular position of mode coupling. To test this, we created two types of terminating layers designed to incorporate specific target molecules (or classes of target molecules). The first type of terminating layer was a commercially available porous polymeric material, and the second type was a mesoporous silicate that was synthesized in the presence of a template to control the size, shape, and polarity of the pores. The incorporation of target molecules within both of these types of materials during a sensing event was expected to alter the RI of the layer and result in a shift in the SEW mode.

3.2.2 Calculated Refractive Index Sensitivity in Polymeric Materials

Because of the strong confinement of the mode in the terminating layer of the PBGM, it was anticipated that very high sensitivity would occur when sensing target molecules diffused into the porous films. Calculations using the methodology developed by Robertson (Shinn, 2005) confirmed the expectation. Using a model film as the outer layer of the PBGM, sensitivity to RI changes was calculated over three orders of magnitude (Figure 12). Due to the narrow reflectivity dips observed with the SEW sensor, changes of these magnitudes can be detected experimentally.

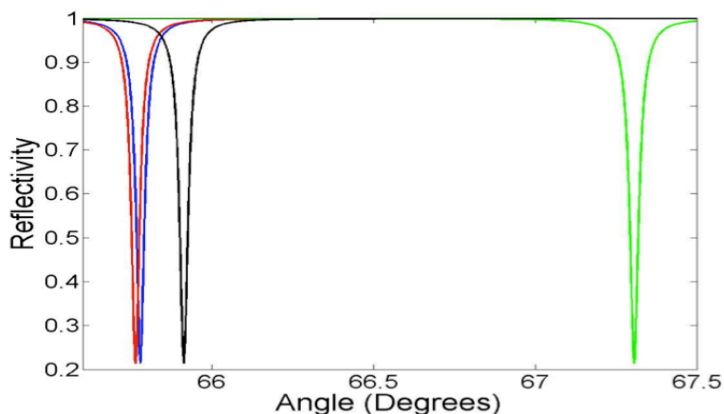


Figure 12. Calculated angular mode shift in a 700 nm thick OV-225 film. The mode (red line) shifts due to 0.01% (blue line), 0.1% (black line), and 1% (green line) changes in RI.

3.2.3 Terminal Layer Design

Organic polymeric materials were used to test the concept that the RI of the terminal PBG layer could be altered. Commercially available Teflon copolymers made from tetrafluoroethylene and 2,2-bis-trifluoromethyl-4,5-difluoro-1,3-dioxole (AF1600 and Teflon AF2400) were chosen because of their porous nature and low RIs (Podgorsek, 1997). Most of the experiments were performed using films spin coated from 3% AF1600 in Fluorinert. Although AF2400 is more commonly used as a porous polymer, the solubility is lower and it required extended periods of sonication to dissolve. Octafluorotoluene was a good solvent for both Teflon copolymers, and this solvent will be used in Phase II experiments.

Another class of compounds, ormosils (organically modified silicates), are mesoporous silicates containing organic ligands that can preferentially solvate organic templates, creating pores of specific size, shape, and polarity upon removal of the template by solvent extraction (Sanchez, 2008). Figure 13 shows how the nitro and aromatic groups in a 2,4-dinitrotoluene (DNT) template can interact with phenyl and methylamino groups in a nanopore. Since thin films of these materials are able to recognize specific enantiomers selectively (Fireman-Shoreh, 2003), the templated pores in the dried films are evidently robust.

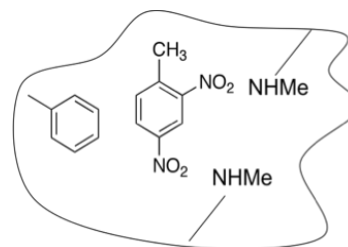


Figure 13. Cartoon showing nanocavity with DNT template.

3.2.4 Ormosil Synthesis

The synthesis of ormosils was accomplished via the sol-gel process, in which tetramethoxysilane, TMOS, (or tetraethoxysilane, TEOS) is hydrolyzed and condensed into a polymeric network, here incorporating organic groups through cocondensation with organotri-alkoxysilanes (Figure 14).



Figure 14. Synthesis of ormosil polymer.

Hybrid sol-gels (Fireman-Shoresh, 2003) containing 20% organic silane (1–5) and 80% inorganic silane were used because the resulting films had favorable properties and could be used to incorporate organic templates to nanoimprint the film with recognition sites. Each sol-gel recipe (Table 3) included aromatic (phenyl) and polar (amine) groups (Figure 15) to solvate the DNT template in the sol-gel environment.

Table 3. Reagents and Conditions for Synthesis of Sol-Gels

Recipe ^a	TMOS (mL)	TEOS (mL)	PTMOS (mL)	HCl (mL)	Silane number/mL	H ₂ O (mL)	Ethanol (mL)	Time (h)
A	2.00	-	0.50	0.66 ^b	1/	0.66	2.00	2
B	2.00	-	0.37	1.00 ^b	2/0.57	1.00	3.00	5
C	-	3.00	0.20	0.10	4/0.17	1.00	3.00	20
D ^c	-	3.00	-	0.10	-	2.00	2.40	2
E	-	3.00	0.20	0.10	3/0.2	1.00	3.00	24
F	2.00	-	0.37	1.00 ^b	5/310.8	1.00	3.00	5

^aBased on Fireman-Shoresh, 2003, unless noted otherwise; ^b0.1 M HCl; ^cbased on Tao, 2007.

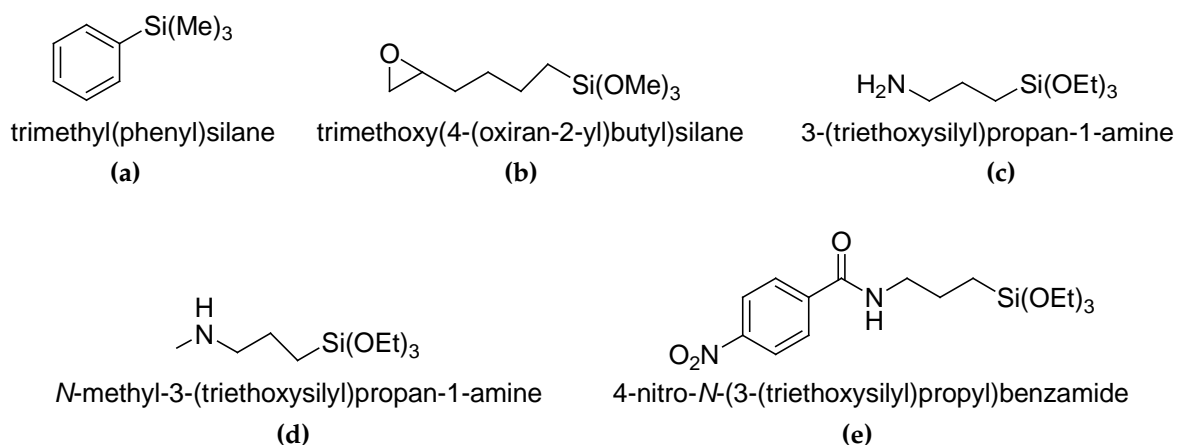


Figure 15. Reagents from Table 3.

The following conditions are typical for an ormosil containing methylaminotriethoxysilane (E): mix 3 mL TEOS, 0.2 mL phenyl trimethoxysilane (PTMOS), 3 mL ethanol, 0.1 mL concentrated HCl, and 0.2 mL 3-aminopropyl trimethoxysilane. This solution was stirred at RT for 24 hours, and then 7.2 mg DNT was mixed with 1.0 mL of the sol-gel solution and stirred for 30 minutes. Conditions for other sol-gel recipes are listed in Table 3.

3.2.5 Substrate Surface Cleaning Method

Before spin coating the terminal layer, all substrates were cleaned using an acid cleaning method to help with film adherence to the substrate. First the slides were placed in an ozone cleaner (Jelight) for 2 minutes per side, then immersed in 1 : 1 HCl-MeOH for 30 minutes, then thoroughly rinsed with water and incubated again in concentrated H₂SO₄ for 30 minutes. The slides were then placed in hot water. A stream of nitrogen was used to thoroughly dry the slides.

3.2.6 Film Formation

An aliquot (40 μ L) of the sol-gel solution containing DNT was spin coated at 4,000 rpm onto silicon (2 in. wafers cut into quarters, Wafer World) or fused silica substrates (1 in. by 1 in. Dell Optics) for 40 seconds to produce thin films. The slides were allowed to dry at RT in a laminar flow hood for 24 hours before the UV spectrum was measured.

3.2.7 Template Removal and Reabsorption

To remove the DNT template, the slides were extracted with methanol (Electronic Grade, Fisher) using a Soxhlet extractor. A UV spectrum was taken every 24 hours or periodically until the DNT was extracted. After DNT extraction, the slides were placed in a screw-cap Teflon jar containing 10 mg DNT for 24 hours for exposure to DNT vapor. UV spectra were taken periodically to detect DNT absorption. Finally the slides were re-extracted with methanol and checked with UV spectroscopy to quantify DNT extraction.

3.2.8 Imprinted Ormosil Characterization

To establish the technique of producing selective nanoimprinted films, the primary characterization method was UV spectroscopy. As shown in Figure 16, the absorbance maximum (λ_{max}) for DNT appears at 252 nm. Because the peak overlaps with the phenyl absorbance in the film, this spectrum is obtained by subtracting a film that is not imprinted with DNT. The film thicknesses were measured using spectroscopic ellipsometry (Woolam M-2000) or by profilometry. Films were typically 600–700 nm thick, with an error of ± 20 nm. SEW mode location in mesoporous silicate films has not yet been successful.

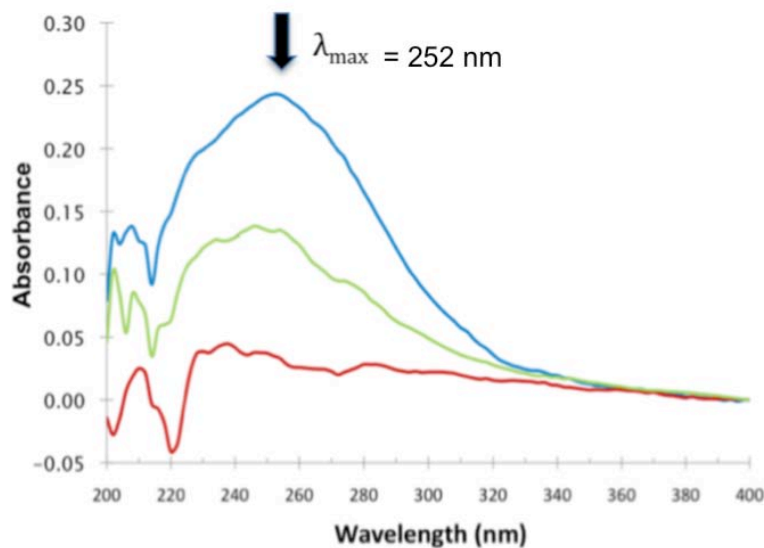


Figure 16. UV spectra of film templated with DNT. The UV spectra are shown for the DNT template film (blue line), after methanol extraction for 24 hours (red line), and after exposure to DNT vapor for 24 hours (green line).

3.2.9 Effect of Film Environment Upon DNT Sensing

Extraction of the DNT template (Figure 17) from films was fastest for inorganic films (D) and those with methylamine groups (C) and slowest for films containing primary amine (E), presumably due to hydrogen bonding interactions between primary amines and DNT. Reabsorption of DNT vapors into extracted films depended on the film environment and was fastest for film D, followed by film C (Figure 18).

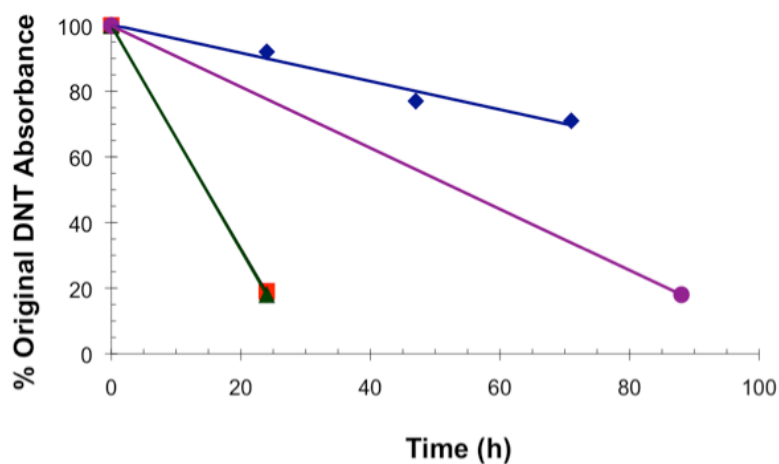


Figure 17. Effect of film environment upon extraction of DNT. The blue points represent DNT in film E (containing primary amine), the purple film B (containing an epoxide), the red and green (overlapping) lines are due to DNT in film C (containing secondary amine) and D (containing no organosilanes), respectively.

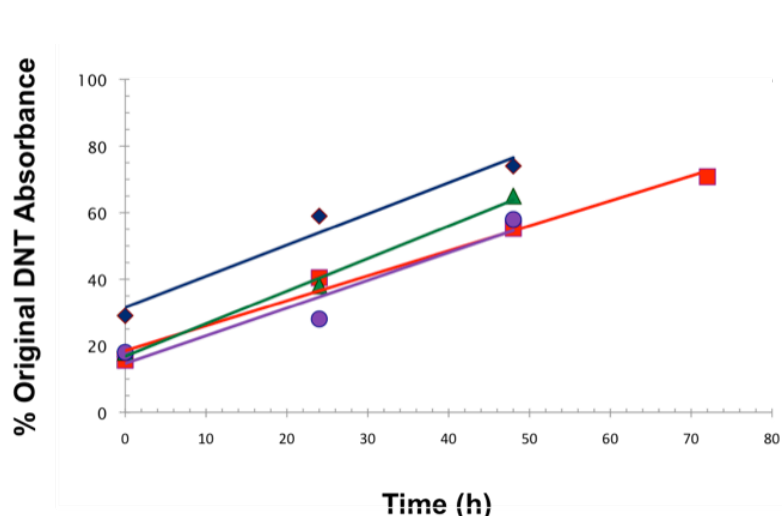


Figure 18. Effect of film environment upon absorption of DNT vapor. The blue points are measured DNT in film E (containing primary amine), the purple points were measured in film B (containing an epoxide), the red points were measured in film C (containing secondary amine), and the green points were measured in film D (containing no organosilanes).

The extraction process is reversible—DNT can be removed, reabsorbed, and re-extracted. Figure 19 demonstrates and compares the reversibility in the four film environments after 24 hours into each procedure.

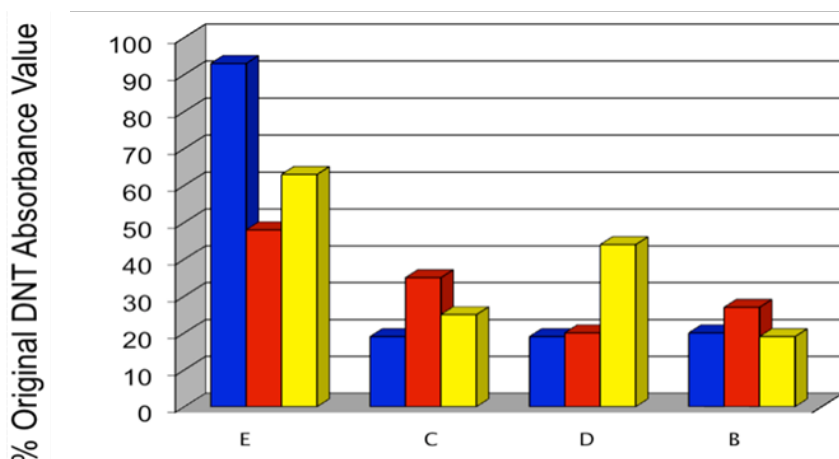


Figure 19. Effect of film environment on percentage of DNT in the film after extraction and reabsorption. The blue bars represent the percentage of DNT left after 24 hours of methanol extraction as compared to original amount of DNT template in the film. The red bars represent percentage of DNT after reabsorption for 24 hours (not correcting for any DNT left in the film). The yellow bars represent the amount of DNT in the film after extraction of the reabsorbed material.

3.2.10 Film Selectivity for DNT

The selectivity of the film for the DNT template was tested by exposing C films to vapors of three additional molecules: 2,4-dimethoxytoluene (DMT), 2,2'-dinitrophenyl (DNB), and 3-nitrophenyl (NB). Spartan (Wavefunction, Inc.) calculations show graphically (Figure 20) that the electrostatic potential density map for DMT has the same shape as that for DNT, but the charge is localized on the outside of the molecule. Both NB and DNB are larger, yet DNB has regions of similar polarity.

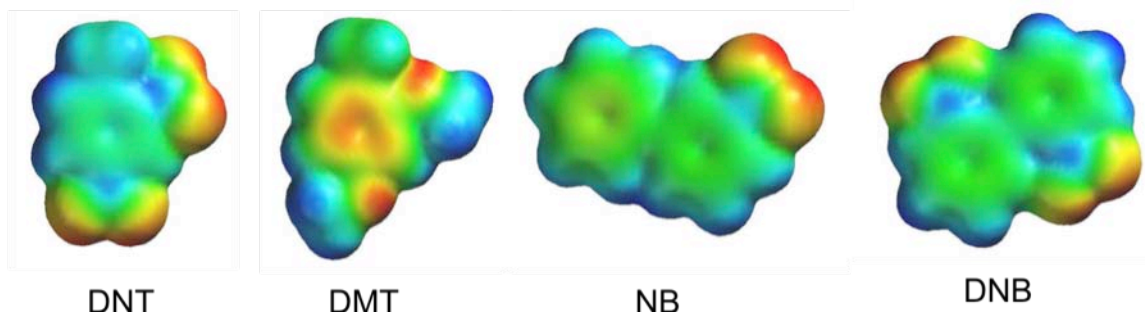


Figure 20. Spartan electrostatic potential density maps for molecules of similar shape (DMT) and polarity (DNB) to DNT.

If shape were the dominating factor, DMT would be expected to be absorbed into the film nanocavities at about the same percentage as DNT. Indeed, DMT was adsorbed at about half the absorbance value of DNT after 3 days, so selectivity is not high. Absorption of neither NB nor DNB was observed, presumably due to low vapor pressures, making a comparison of selectivity between the three compounds inconclusive.

3.2.11 Nonselective Gas and Vapor Sensing with the SEW Sensor

We accomplished a number of advances during this part of the research project. We made the first measurements to show that the SEW sensing platform could be used to detect gases and vapors without a specific preference for one type of molecule (nonselective), and we demonstrated that it is possible to apply a sensing layer by spin coating. The presence of a porous sensing layer leads to much higher sensitivity, and this finding will be pursued further in Phase II.

In the gas sensing experiments that we conducted to demonstrate the feasibility of this system we typically detected organic vapors that were carried through the flow cell using a transport gas such as nitrogen or air. Typical results with four different organic vapors are shown in Figure 21. The vapors from left to right are isopropanol, acetone, acetic acid, and ether. There is a signature associated with each vapor that could possibly be used to identify species.

We also measured the response of pure gases directly. We were clearly able to distinguish air, carbon dioxide, helium, and various other gases. These gases differ in RI by only a few parts per 10,000, demonstrating the sensitivity of the SEW resonance technique.

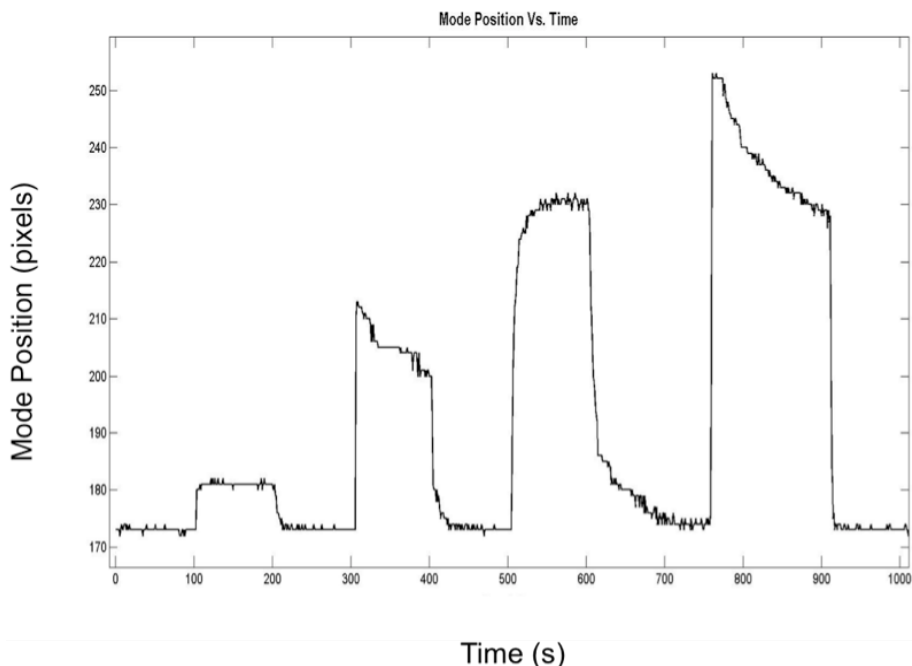


Figure 21. Vapor binding results for isopropanol, acetone, acetic acid, and ether (left to right).

3.3 Develop Strategies for Compact Sensors (Task 3)

Work on engineering a compact portable version of the device centered on determining a suitable laser source with sufficient stability that could be run on a battery power source. We had done most of our preliminary experiments using a HeNe laser. These lasers are stable in terms of power and wavelength; however, they are not compact. For this project we switched to using a diode laser at 635 nm that was coupled to a single-mode fiber. The use of the fiber was a benefit in that hardware for steering a free-space beam to the prism was eliminated. However, the diode laser was not sufficiently wavelength stable. There were small mode hops that shifted the wavelength of the source, which resulted in a concomitant shift in the coupling angle. This effect led to significant noise in our sensing data. For the most precise experiments we returned to the use of the HeNe laser. Near the end of the project we identified a new wavelength stabilization technology based on volume holographic gratings that permits diode lasers to have stability on a par with HeNe lasers. We have purchased one of these lasers, and we will test it as a source for the next phase of the project.

The basic configuration of a compact (shoe-box sized) version of the sensor is shown in Figure 22. The benchtop version that has been used for the experiments of this phase of the project is essentially as shown in the schematic except that we do not have a box enclosure and we are running off of plug power rather than battery power.

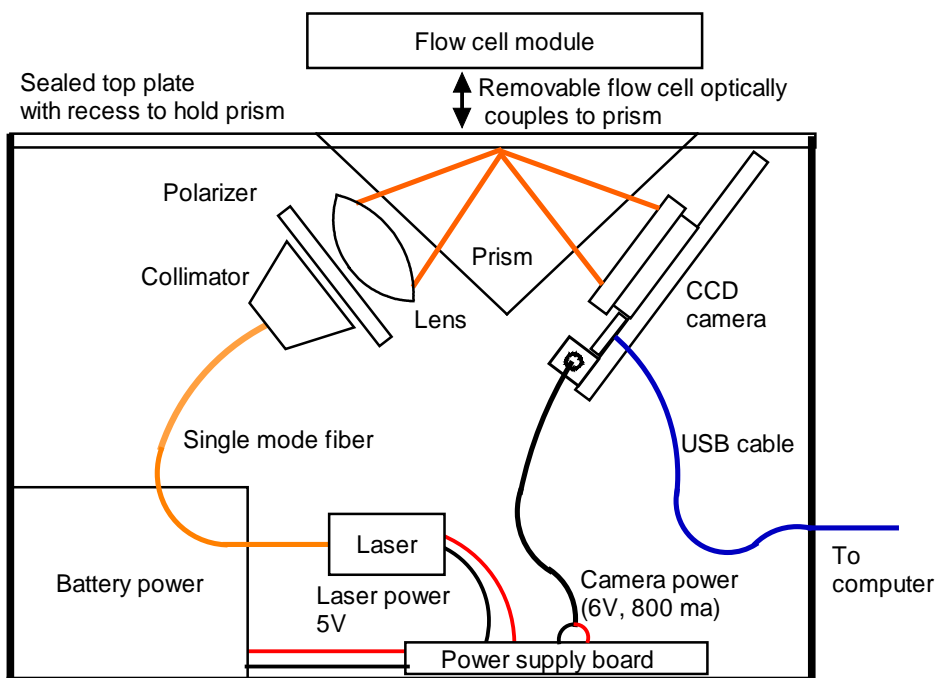


Figure 22. Schematic of a compact portable SEW sensor configuration.

3.4 Quantification of Sensitivity

The question of comparing sensitivity of detection techniques for biological and chemical entities is a complicated and subtle subject. A technique that may appear to be very sensitive via one metric, such as RI determination, may not prove to be nearly as sensitive to surface binding events necessary for the detection of biological substances such as spores and proteins. In this brief overview we will compare the SEW sensing technique to SP sensing.

SP sensing is the standard in terms of high sensitivity, real-time sensing methods. There are biological methods such as polymerase chain reaction for detection, but these typically take hours or days (Makino, 2001) and thus are not a relevant point of comparison for a technique such as SEW that is designed to work in a much shorter time frame.

One standard method for comparing the sensitivity of the SP sensing technique is to measure the shift in the SP coupling angle with the change in RI of the solution in contact with the metal film. Typical values for the SP sensitivity by this measure are 50–100° per RI unit (/RIU). In other words the SP will shift between 50 and 100 degrees if the RI of the solution changes by 1. The corresponding value for the SEW method using this metric is 25–40°/RIU, which makes it appear that the SEW technique is less sensitive to RI. However, this simple angle shift definition does not account for the fact that the width of the SEW resonance is about 100 times narrower than the SP resonance in gold. For comparing SP devices the resonance width is always essentially the same and is determined by the optical properties of gold. If the resonance width is factored in, the SEW technique is about 50 times more sensitive than SP sensing for RI measurements.

Although RI is a convenient method for measuring and comparing the performance of sensors, the result has very little to do with the ultimate sensitivity to biosensing reactions in which a small molecule such as a protein binds to the surface of the sensor. In this case the

RI of the solution remains relatively stable—the only disturbance of the resonance condition is due to the presence of the bound molecule in the few nanometers above the surface of the sensor. The shift in resonance in this case comes from the overlap of the decaying evanescent field of the surface wave (SP or surface optical wave) and the dielectric modulation due to the bound biomolecule. Larger shifts in surface wave resonance occur if the evanescent field decay length matches the approximate size of the molecule. For SP sensors the primary technique to vary the evanescent field decay length is changing wavelength. Prism material can also affect this distance making a realistic comparison of SP sensors amongst themselves a very difficult matter (example <http://www.biosensingusa.com/Application102.html>). In this regard the SEW sensor has a unique advantage in that the evanescent field penetration distance can be engineered by an appropriate design of the multilayer. The values of penetration depth for SEWs are typically less than for SPs, thus the SEW technique is particularly suited to biodetection.

The foregoing discussion demonstrates that because there are so many adjustable parameters and variables it is a very difficult task to give one simple metric that validly compares SP and SEW sensing. We are confident in general terms that the SEW sensor has higher sensitivity than SP sensors in real-world testing scenarios—in particular because it can be engineered to exhibit optical properties tailored to a particular target. Because of the complexity of detailed comparisons, the approach we are adopting is to construct a SEW sensor that is optimized for a given target or set of targets and let any comparison be made by experts in other competing sensing techniques when we publish our results.

4. SUMMARY

The key deliverable in the statement of work was the demonstration of sensitivity, speed, specificity, and reproducibility of the SEW flow sensor. Measures of sensitivity include the detection of gases differing by 1 in 10,000 RI values (Figure 20) and a 20 pixel shift in SEW mode in response to spore-antibody binding in solution. Solution and gas measurements are made in real time and are therefore rapid—limited only by diffusion rates, concentration, and binding strength. Measures of specificity include the fluorescence detection of selective binding of endospore anthrax models to antibodies and two stages of affinity binding of spore and antibody (Figure 10) that were confirmed by fluorescence experiments. The SEW sensor is more robust and versatile and as easy to use as commercial SP resonance instruments due to the availability of commercially fabricated PBGMs with a chemical binding layer. For gas sensing, the PBGM is also commercial, and spin-coated terminal layers are easily applied for specific applications. Difficulties in reproducibility of biosensing arise from the complexity of applications under development, and false positives are due to nonspecific binding rather than inherent problems with the technique. Gas sensing is very reproducible and tolerant of conditions.

5. REFERENCES

Buckeridge, DL; Owens, DK; Switzer, P; Frank, J; and Musen, MA. 2006. Evaluating detection of an inhalational anthrax outbreak. *Emerg Infect Dis.* 12: 1942–1949.

Carrera, M; Zandomeni, RO; Fitzgibbon, J; and Sagripanti, JL. 2006. Difference between the spore sizes of *Bacillus anthracis* and other *Bacillus* species. *J Appl Microbiol.* 102: 303–312.

- Cieslak, TJ, and Eitzen, Jr., EM. 1999. Clinical and epidemiologic principles of anthrax. *Emerg Infect Dis.* 5: 552–555.
- Elias, B. "Air Cargo Security," CRS Report for Congress, July 30, 2007.
- Fireman-Shoresh, S; Avnir, D; and Marx, S. 2003. General method for chiral imprinting of sol-gel thin films, exhibiting enantioselectivity. *Chem. Mater.* 15: 3607–3613.
- Image J: Image Processing and Analysis in Java. National Institutes of Health. (<http://rsb.info.nih.gov/ij/>).
- Joklik, WK; Willett, HP; Amos, DB; and Wilfert, CM. 1988. *Zinsser Microbiology*, 19th ed. Norwalk: Appleton & Lange.
- Makino, SI; Cheun, HI; Watarai, MI; Uchida, M,; and Takeshi, K. 2001. *Lett. Appl Microbiol.* 33: 237–240.
- Podgorsek, RP; Sterkenburgh, T; Wolters, J; Ehrenreich, T; Nischwitz, S; and Franke, H. 1997. Optical gas sensing by evaluating ATR leaky mode spectra. *Sensors and Actuators B.* 38–39: 349–352.
- Quinlan, JJ, and Foegeding, PM. 1997. Monoclonal antibodies for use in detection of *Bacillus* and *Clostridium* spores. *Appl Environ Microbiol.* 63: 482–487.
- Robertson, WM. 2008. US Utility Patent #7,436,596. Optical sensor based on surface electromagnetic wave resonance in photonic band gap materials and method for using same.
- Shinn, M; and Robertson, WM. 2005. Surface plasmon like sensor based on surface electromagnetic waves in a photonic band gap material. *Sensors and Actuators B.* 105: 360–64.
- Sanchez, C; Boissiere, C; Grosso, D; Laberty, C; and Nicole, L. 2008. Synthesis and properties of inorganic and hybrid thin films having periodically organized nanoporosity. *Chem. Mater.* 20: 682–737.
- Tao, S, and Li, G. 2007. Porphyrin-doped mesoporous silica films for rapid TNT detection. *Colloid Poly. Sci.* 285: 721–728.